Available online at www.sciencedirect.com
ScienceDirect
Ceramics International 37 (2011) 1251–1257
CERAMICS INTERNATIONAL
www.elsevier.com/locate/ceramint

Synthesis of high surface area Al_2O_3–CeO_2 composite nanopowder via inverse co-precipitation method

S.A. Hassanzadeh-Tabrizi, E. Taheri-Nassaj *

Department of Materials Science and Engineering, Tarbiat Modares University, PO Box 14115-143, Tehran, Iran

Received 30 August 2010; received in revised form 14 October 2010; accepted 1 December 2010
Available online 21 January 2011

Abstract

In the present work, Al_2O_3–CeO_2 composite nanopowder was synthesized by inverse co-precipitation method using metal chlorides, aluminum powder and NH_4OH as precipitant agent. The thermal decomposition of the precipitate and subsequent formation of Al_2O_3–CeO_2 were investigated by X-ray diffractometery, scanning electron microscopy, thermogravimetric and differential thermal analysis, Brunauer–Emmett–Teller surface area measurement and Fourier transform infrared spectroscopy. The results showed that the presence of ceria suppressed the formation of α-Al_2O_3. The BET-specific surface area was 173 m^2/g for powders calcined at 800 °C. The particle size examined by using scanning electron microscopy was in the range 30–70 nm. The activation energy of Al_2O_3–15 wt.% CeO_2 nanocrystallite growth during calcination was measured to be 32.4 kJ/mol whereas that of Al_2O_3 was about 23.8 kJ/mol.

Keywords: Composites; Nanostructures; Chemical synthesis; X-ray diffraction

1. Introduction

Nanoscale composite materials in the form of powders, spheres, fibers, tubes, and coatings have attracted a great deal of interest in diverse fields, because of their unexpected and unprecedented properties, which are unattainable in normal materials. When more than two different phases are organized, the performance of the whole system is significantly influenced by their organization level [1–3]. Nowadays, the ceria–alumina supported system constitutes one of the most widely used mixed-oxides for elimination of pollutants in automobile exhaust gases [4]. The Ce^{3+}/Ce^{4+} oxidation–reduction properties make cerium a good promoter for the combustion reaction due to its capacity to deliver oxygen [5]. In nano-scale form, as the particle size decreases, the amount of lattice defects, such as oxygen vacancies and grain boundary increases. Moreover, high surface area increases the catalytic efficiency of these inorganics [6]. As it is known synthesis route has an important effect on properties of products. Conventional processes for synthesizing ceramic nanopowders involve mechanical synthesis [7], vapor deposition [8], precipitation [9], combustion [10], sol–gel [11], hydrothermal and solvothermal synthesis [12,13], and other related methods. Among these methods, chemical processes produce fine particles of high purity and high specific surface area. In addition chemical processes achieve intimate mixing of reactant cations on the atomic level, leading to an increase in reaction rate and lowering synthesis temperature. For instance, sol–gel method is the most widely employed chemical route to mixed metal oxides, and it has the apparent advantages of lower heat-treated temperature. However, it also has some disadvantages, such as the pH control, expensive starting materials and long reaction time. The hydrothermal and solvothermal synthesis can avoid the problems described above. However, hydrothermal synthesis requires complicated and expensive facilities due to the higher operating temperatures and pressures. Compared with these methods, homogeneous precipitation method is one of the most promising techniques because of the inexpensive starting materials, a simple synthesis process and commonly available apparatus. In the present work, an alumina–ceria composite nanopowder was synthesized through a reverse strike precipitation method using metal salts, aluminum powder and NH_4OH as precipitant agent. This method has the advantages of low processing cost and homogeneity of

* Corresponding author. Tel.: +98 21 82883306; fax: +98 21 88005040.
E-mail address: taheri@modares.ac.ir (E. Taheri-Nassaj).

0272-8842/$36.00
doi:10.1016/j.ceramint.2010.12.004

product. Decomposition of the precipitate, phase transformation, surface area and morphology of the synthesized alumina–ceria powder were investigated.

2. Experimental procedure

The precursor solutions for Al_2O_3–15 wt.% CeO_2 nanopowder were prepared by inverse co-precipitation method (so-called reverse-strike) using $AlCl_3{\cdot}6H_2O$ (Merck), Al powder, $CeCl_3{\cdot}7H_2O$ (Merck), HCl (Merck) and NH_4OH (Merck). The aluminum powder was produced by M.A. University. This powder has a spherical shape with an average diameter about 37.5 μm. In the inverse co-precipitation method, the cation solution is added to the precipitation solution. This technique leads to better homogeneity of the precursor for multication materials [14]. First $AlCl_3{\cdot}6H_2O$ and $CeCl_3{\cdot}7H_2O$ were dissolved in deionized water and HCl. Then aluminum powder was added to the solution. The precursor solution was continuously stirred at 100 °C for 4 h to completely dissolve the starting materials. The solution was added drop-wise to NH_4OH while keeping a constant pH value of 9 by adding extra-ammonia solution, under continuous monitoring by a pH-meter to allow very small pH fluctuations (±0.2 pH units). The obtained precipitate was washed using distilled water to remove the impurities, and finally dried at 80 °C for 48 h. The obtained dried precipitate was ground into powder, and then the powder was calcined in a muffle furnace at different temperatures. The flow chart of the powder preparation is shown in Fig. 1. In order to study the effects of ceria on the phase transformations in the precipitate, a specimen was prepared without ceria according to the above procedure.

X-ray diffraction (XRD) was carried out for phase analysis of the dried precipitate and calcined powder using Philips X-pert model with CuKα radiation. The average crystallite size (d) of the powder was estimated from the Scherrer equation (Eq. (1)):

$$d = \frac{0.9\lambda}{\beta_{\text{sample}} \cos(\theta)} \tag{1}$$

where λ is the wavelength, θ is the diffraction angle, and β_{sample} is the full-width for the half-maximum (FWHM) intensity peak of the powder. For instrumental correction, the Gaussian–Gaussian relationship (Eq. (2)) was used:

$$\beta^2_{\text{sample}} = \beta^2_{\text{exp}} - \beta^2_{\text{ins}} \tag{2}$$

where the measured FWHM of the powder is shown by β_{exp} and that of the standard sample is indicated by β_{ins}. Differential thermal analysis (DTA) and thermogravimetric (TG) were used in the range of 25–975 °C with a rate of 10 °C/min with the STA equipment (PL Thermal Sciences STA 1500, U.K.). N_2 adsorption–desorption isotherms were determined in a surface analyzer equipment (BEL Japan Inc., Osaka, Japan) at 77 K. BET surface area and BJH analyses were used to determine the total specific surface area and the pore size distribution. The powder morphology was investigated using a Phillips XL30 scanning electron microscope (SEM). Fourier transform infrared (FTIR) spectroscopy analyses of dried precipitate and calcined powders were carried out in a Nicolet Nexus 6700 for studying the chemical groups of the dried precipitate and calcined powders.

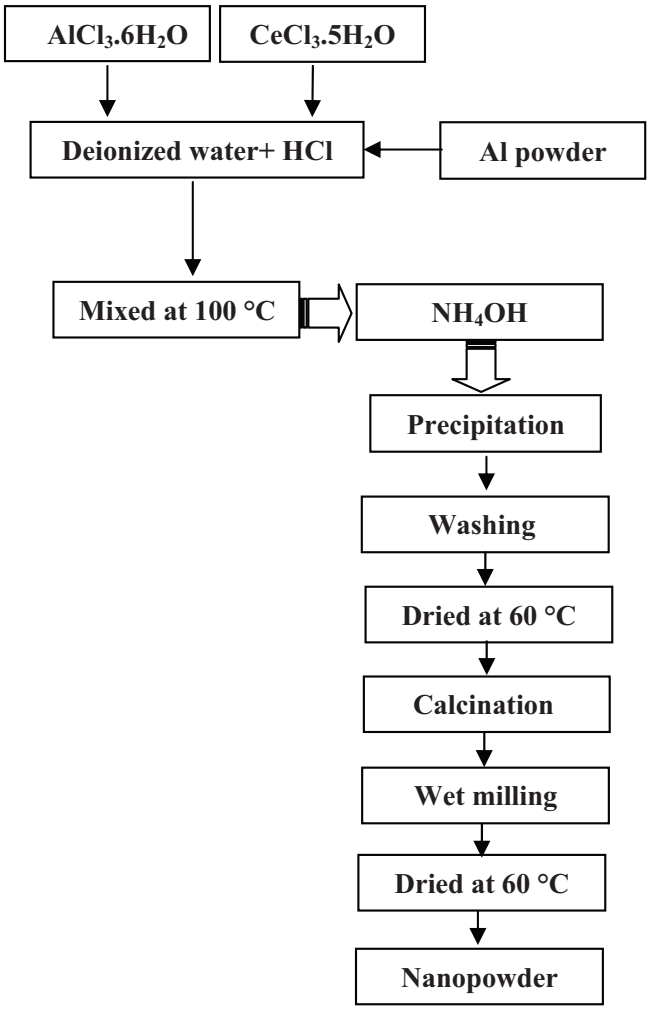

Fig. 1. The flow chart of the processing of Al_2O_3–CeO_2 nanopowder.

3. Results and discussion

The synthesis mechanism may be described by the following reactions. Reaction (R1) shows that Al powder reacts with HCl to produce aluminum chloride and therefore Al can be used as a source of $AlCl_3$.

$$2Al + 6HCl \rightarrow 2AlCl_3 + 3H_2 \tag{R1}$$

A precipitate is obtained by adding NH_4OH to aluminum chloride hexahydrate solution (reaction (R2)). The precipitation is due to the low solubility of $Al(OH)_3$ (25 °C. $K_{sp} = 1.3 \times 10^{-33}$)

$$AlCl_3 + 6NH_4OH \rightarrow 2Al(OH)_3 + 3NH_4Cl \tag{R2}$$

At ageing step $Al(OH)_3$ converts to crystalline boehmite by reaction (R3) [15,16].

$$Al(OH)_3 \rightarrow AlOOH + H_2O \tag{R3}$$

Transition alumina is produced by the calcination of dried boehmite (reaction (R4)).

$$AlOOH \rightarrow Al_2O_3 + H_2O \quad (R4)$$

The formation of cerium hydroxide occurs by reaction (R5) in solution at a high pH with subsequent precipitation of $Ce(OH)_3$ (25 °C, $K_{sp} = 6.3 \times 10^{-24}$).

$$CeCl_3 + 3NH_4OH \rightarrow Ce(OH)_3 + 3NH_4Cl \quad (R5)$$

The oxidation of $Ce(OH)_3$ to $Ce(OH)_4$ also occurs in air at room temperature [17]. Then the precipitate dehydrates progressively and forms CeO_2 (reaction (R6)).

$$CeO_2 \cdot 2H_2O \rightarrow CeO_2 \cdot (2-n)H_2O + nH_2O \quad (R6)$$

With respect to, aluminum powder is cheaper than aluminum chloride hexahydrate, therefore, it is desirable to increase the $Al/AlCl_3 \cdot 6H_2O$ ratio. The influence of the weight ratio of $Al/AlCl_3 \cdot 6H_2O$ on the color of the resulting solutions is summarized in Table 1. As can be seen, increasing the amount of aluminum content in the solution decreases its transparency. Evidently this is due to insufficient solubility of aluminum in the solution. It seems that the 0.2 wt.% of $Al/AlCl_3 \cdot 6H_2O$ is an optimum ratio. The molar ratio of HCl/H_2O should be fixed at about 0.18 to form a solution. The appearance of solution would be opaque or translucent when the ratio of HCl/H_2O is lower than 0.18 due to insufficient amount of acid for dissolving of aluminum powder. Adding more acid than 0.18 would result in instability of solution which may be due to the catalytic effect of HCl.

Fig. 2 presents thermogravimetry and differential thermal analysis (TG–DTA) curves of the dried precipitated powder. The DTA curve shows two endothermic peaks at 75 and 279 °C which are attributed to evaporation of absorbed water and dehydration of the dried precipitate, respectively. In addition a small endothermic pick at 420 °C may be attributed to the remaining hydroxyl groups in the precipitate. TG curve shows an overall weight loss of approximately 28% up to 590 °C and reveals less change at higher temperature, which can be attributed to the removal of molecular water and dehydration of the precipitate. No significant weight loss occurs after 700 °C. The total weight loss of 31% appears in the precipitate.

The X-ray diffraction patterns of the precipitate heat treated for 3 h at temperature ranges from 60 to 1200 °C are shown in Fig. 3. As can be, the dried precipitate consists of CeO_2 with pure cubic structure and AlOOH (boehmite). By increasing the heat treatment temperature to 400 °C, boehmite changes to

Table 1
Dependence of weight ratio of $Al/AlCl_3$ on solution formation.

Weight ratio of $Al/AlCl_3$	Molar ratio of H_2O/Al	Solution description
0.10	30	Transparent
0.12	30	Transparent
0.14	30	Transparent
0.16	30	Transparent
0.20	30	Transparent
0.25	30	Translucent (not suitable)
0.50	30	Opaque (not suitable)

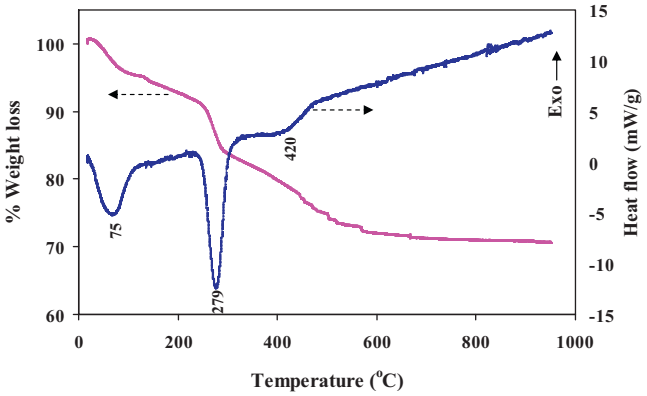

Fig. 2. DTA and TG curves of the precipitate.

amorphous alumina according to reaction (R4) and only the ceria peaks are detected. Amorphous alumina converts to η-Al_2O_3 at 600 °C. By increasing the temperature to 1100 °C, θ-Al_2O_3 is formed. The peak intensity of these phases (CeO_2, η-Al_2O_3 and θ-Al_2O_3) increases with increasing the temperature. In addition the broadening of the peaks decreases which shows growing the nanocrystallites. Transformation of transition phases of alumina to α-Al_2O_3 takes place at 1200 °C. Some researchers reported that [18,19], $CeAlO_3$ (cerium aluminate) is formed during heat treatment of this composite but in our work there was no evidence about the formation of $CeAlO_3$ compound. It was reported that $CeAlO_3$ is formed under reducing conditions [20]. During the reduction of the Al_2O_3–CeO_2 composites the cerium ion is reduced from 4^+ to 3^+ state. Consequently, new types of interaction between these ions and alumina can be considered to form cerium aluminate. In this work, the specimens were not under reducing conditions and therefore cerium aluminate was not formed.

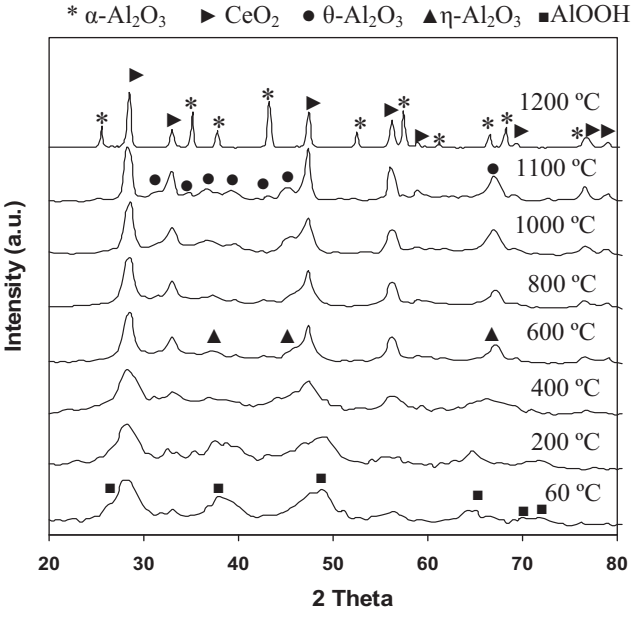

Fig. 3. The XRD patterns of composite samples heat treated at various temperatures for 3 h.

The XRD patterns of pure alumina precipitate without cerium oxide are shown in Fig. 4. It shows the presence of crystalline boehmite as the only crystalline phase in the dried precipitate. By increasing the temperature, boehmite is totally converted into η-alumina at 600 °C. In the range from 800 °C to 1000 °C, η and θ-alumina are the identified phases and the intensity of their corresponding peaks increases with increasing the temperature. As temperature increases to 1100 °C, α-alumina appears.

It can be concluded that from the XRD patterns shown in Figs. 3 and 4 the presence of ceria suppresses the formation of α-Al_2O_3. The formation of α-alumina from transitional aluminas involves the rearrangement of the oxygen lattice from a more or less distorted cubic array to a hexagonal close packed structure. After this transformation, the cations occupy the octahedral sites and there is an increasing ordering of the cation vacancies. As α-alumina forms by a nucleation and growth process, spherical colonies of α-alumina nucleate in a porous matrix of transitional aluminas and grow gradually via the coarsening process. Higher amounts of cations can be dissolved in transitional aluminas than in α-alumina because of the cubic spinel structure with a considerable number of defects and disorder [21]. During the transformation of α-alumina, the ceria comes out of the cubic lattice sites and enters the interstitial and vacant lattice sites causing expansion of the lattice along the *a*-axis. These cerium ions preferably exert dragging force on the diffusion of aluminum ions and hence the transformation to α-alumina occurs at higher temperatures in the presence of ceria.

The average crystallite size of pure Al_2O_3 and Al_2O_3–CeO_2 powder as a function of calcination temperature is shown in Fig. 5. The average crystallite size of all powders increases, by increasing calcination temperature. Increasing of crystallite size is attributed to typical effect of temperature on crystal growth. In addition the crystallite size of Al_2O_3 with 15 wt.% CeO_2 ceria is smaller than pure Al_2O_3. It is evident that CeO_2 addition inhibits crystal growth of alumina. Straight line of ln(*D*) against 1/*T* is plotted in Fig. 6 according to the Scott equation, given below on the assumption that the nanocrystallite growth is homogeneous [22], which approximately

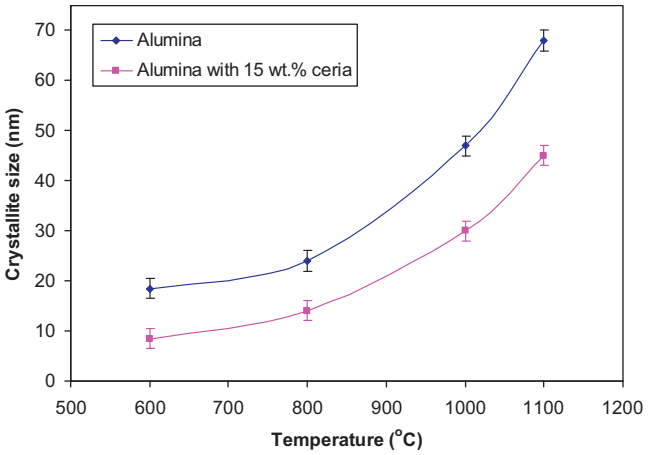

Fig. 5. Effect of calcination temperature on crystallite size.

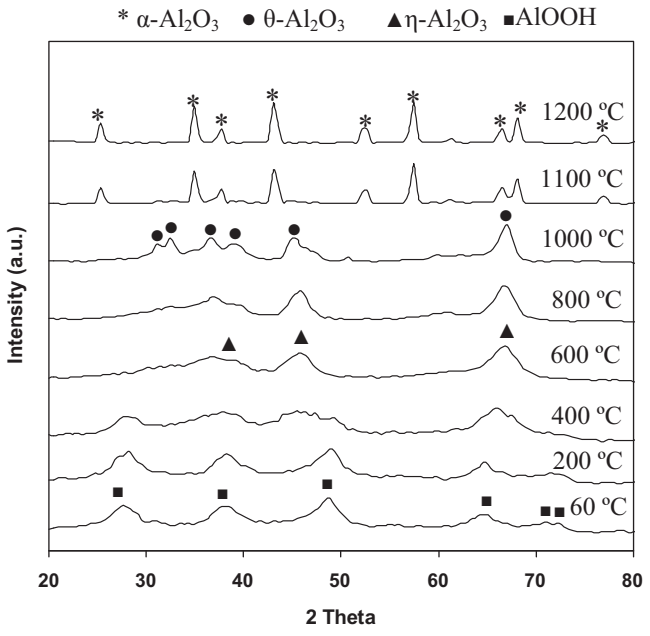

Fig. 4. The XRD patterns of pure alumina precipitate heat treated at various temperatures for 3 h.

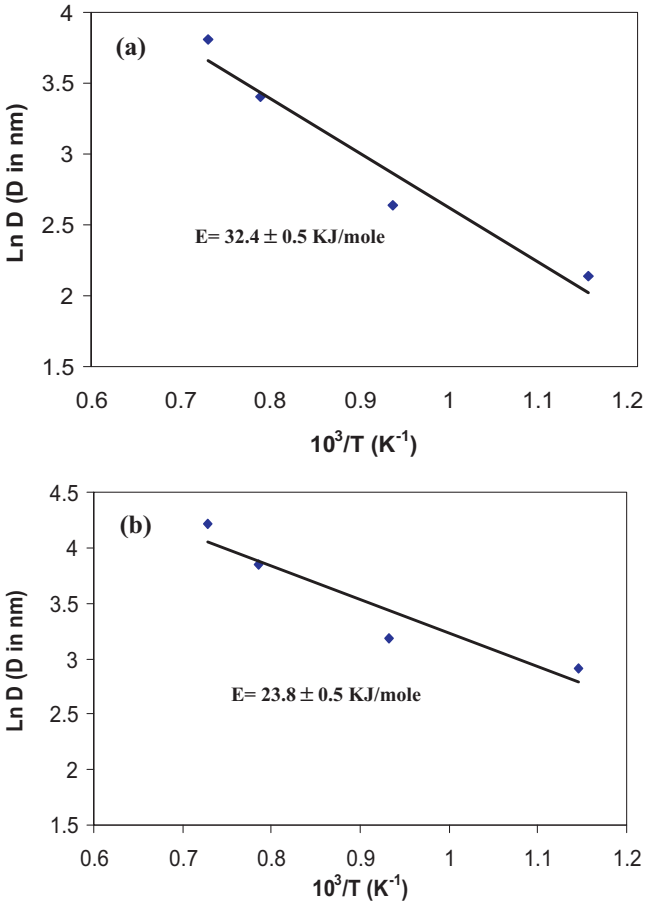

Fig. 6. The plot of ln(*D*) versus 1/*T* for the calculation of activation energy (*E*) for (a): alumina with 15 wt.% ceria and (b):alumina.

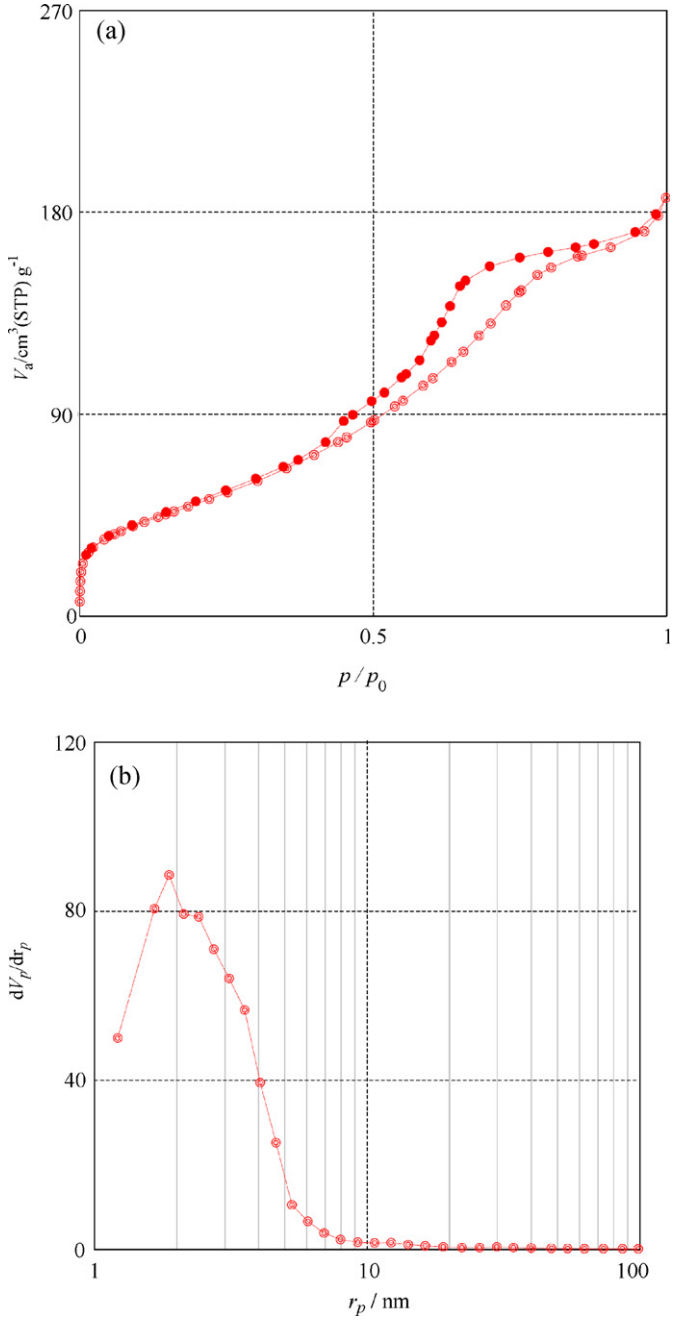

Fig. 7. (a) Nitrogen adsorption–desorption isotherm at 77 K and (b) BJH pore size distribution of powders calcined at 800 °C.

describes the nanocrystallite growth during annealing:

$$D = C\exp\left(\frac{E}{RT}\right)$$

where D is the crystallite size, C is the constant, E is the activation energy for nanocrystallite growth, R is the ideal gas constant and T is the absolute temperature of heat treatment. The activation energies of alumina and alumina with 15 wt.% ceria during calcination were measured about 23.8 and 32.4 kJ/mol, respectively. It clearly shows that adding ceria increases the activation energy for crystallite growth of alumina and can cause a delay in crystal growth.

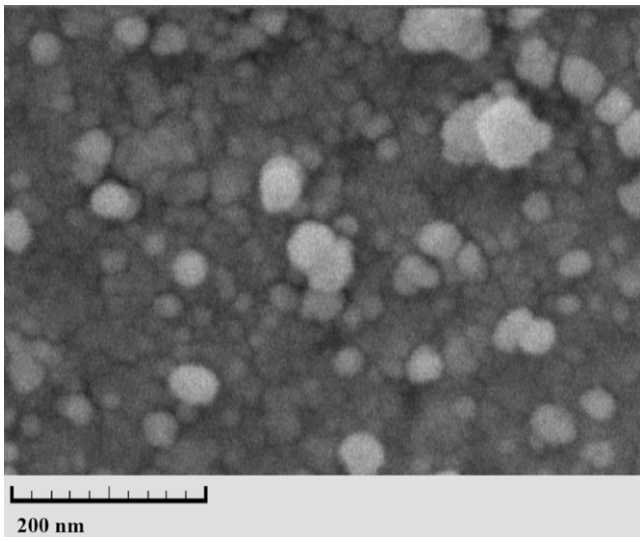

Fig. 8. Scanning electron micrograph of Al_2O_3–15 wt.% CeO_2 powder after heat treatment at 800 °C.

The nitrogen adsorption–desorption isotherm at 77 K and the BJH pore size distribution of sample calcined at 800 °C are shown in Fig. 7. It can be observed that the powder exhibits the classical shape of a type IV isotherm according to the IUPAC classification, typical for mesoporous solids [23]. The existence of the hysteresis loop in the isotherms is due to the capillary condensation of N_2 gas occurring in the mesopores. The surface area and the mean pore diameter of powder calcined at 800 °C are 173 m^2/g and 6.4 nm, respectively.

Fig. 8 shows the SEM image of the powders heat treated at 800 °C. Most of the particles are in the range of 30–70 nm and spherical in shape. In inverse precipitation, because the rate of nucleation is much faster than the rate of particle growth, the resultant precursor particles are very fine, as is shown in Fig. 8. This could be explained by the famous LaMer diagram [24] shown in Fig. 9. It is clear that the nucleation rate is strongly dependent on the supersaturation ratio, the ratio of the

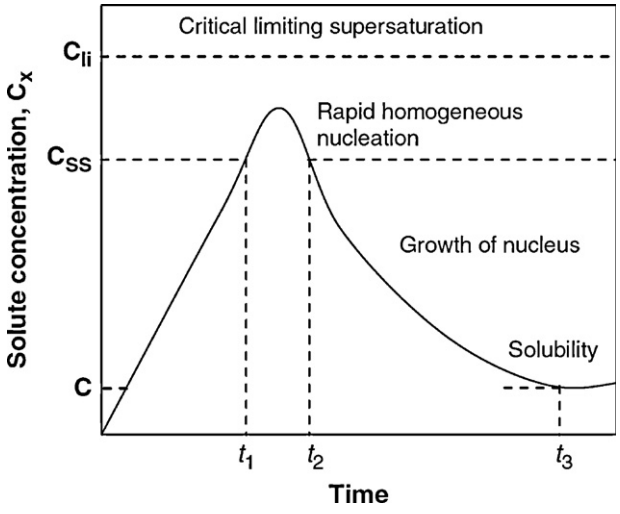

Fig. 9. LaMer diagram.

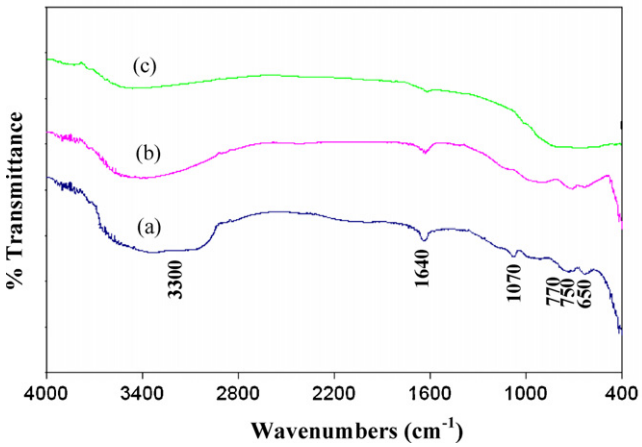

Fig. 10. IR spectra of Al_2O_3–15 wt.% CeO_2 powder heat treated at various temperatures:
(a) 60 °C; (b) 250 °C; (c) 400 °C.

supersaturation concentration to the saturation concentration, C_{SS}/C_S. In inverse precipitation, a sharp increase in C_{SS}/C_S results in a short burst of nucleation that occurs in a shortened time interval, $t_2 - t_1$, and the time interval of nucleus growth, $t_3 - t_2$, is also shortened, because the solute is largely consumed in the nucleation stage. Therefore nanosized powders are formed in this method.

Fig. 10 represents the Fourier transform infrared (FTIR) spectroscopy spectra of the alumina Ceria powder heat-treated at various temperatures for 3 h. The absorption broad peak at 3000–3600 cm^{-1} [25] and absorption peak at around 1640 cm^{-1} [26] correspond to the ν(O–H) and δ(O–H) vibration of water, respectively. The two absorption peaks become weaker by increasing the heat treatment temperature. The absorption peak around 1070 cm^{-1} [27] in the precipitate heat treated at 80 °C corresponds to Al–OH bonding mode. As can be seen this peak disappears by increasing the heat treatment temperature at 250 °C. The broad overlapping peaks in the lower frequency range (500–1000 cm^{-1}) are owing to the presence of Al–O (788.34 and 690 cm^{-1} [28]) and Ce–O (770 cm^{-1} [29]) infrared vibrations, respectively.

4. Conclusions

In the present study an Al_2O_3–CeO_2 nanopowder was synthesized via an inverse co-precipitation method using $AlCl_3{\cdot}6H_2O$, $CeCl_3{\cdot}7H_2O$, Al powder. The total weight loss of 31% appeared in the precipitate after heat treatment at 700 °C. The dried precipitate consisted of CeO_2 with pure cubic structure and AlOOH. The precipitate transformed to Al_2O_3–CeO_2 at higher temperatures. The presence of ceria suppressed the formation of α-Al_2O_3. The BET-specific surface area was 173 m^2/g for powders calcined at 800 °C. Most of the particles heat treated at 800 °C were in the range of 30–70 nm and spherical in shape. The activation energy of Al_2O_3–15 wt.% CeO_2 nanocrystallite growth during calcination was measured to be 32.4 kJ/mol whereas that of Al_2O_3 was about 23.8 kJ/mol.

References

[1] S. Komarneni, Nanocomposites, J. Mater. Chem. 2 (1992) 1219–1230.
[2] H. Gleiter, Nanocrystalline materials, Prog. Mater. Sci. 33 (1989) 223–315.
[3] S.A. Hassanzadeh-Tabrizi, E. Taheri-Nassaj, Effects of milling and calcination temperature on the compressibility and sinterability of a nanocrystalline Al_2O_3–$Y_3Al_5O_{12}$ composite powder, J. Am. Ceram. Soc. 91 (2008) 3546–3551.
[4] G.D. Angel, J.M. Padilla, I. Cuauhtemoc, J. Navarrete, Toluene combustion on γ-Al_2O_3–CeO_2 catalysts prepared from boehmite and cerium nitrate, J. Mol. Catal. A: Chem. 281 (2008) 173–178.
[5] J.M. Padilla, G. Del-Angel, J. Navarrete, Improved Pd/γ-Al_2O_3–Ce catalysts for benzene combustion, Catal. Today 133–135 (2008) 541–547.
[6] J. Chandradass, M. Balasubramanian, D. Bae, K.H. Kim, Effect of different fuels on the alumina–ceria composite powders synthesized by sol–gel auto combustion method, J. Alloys Compd. 479 (2009) 363–367.
[7] K. Han, T. Ko, Synthesis and phase formation of ferroelectric $Bi_4Ti_3O_{12}$ nanopowder by mechanical alloying, J. Alloys Compd. 473 (2009) 490–495.
[8] P. Singh, A. Kumar, Deepak, D. Kaur, ZnO nanocrystalline powder synthesized by ultrasonic mist-chemical vapour deposition, Opt. Mater. 30 (2008) 1316–1322.
[9] K. Maaz, S. Karim, A. Mumtaz, S.K. Hasanain, J. Liu, J.L. Duan, Synthesis and magnetic characterization of nickel ferrite nanoparticles prepared by co-precipitation route, J. Magn. Magn. Mater. 321 (2009) 1838–1842.
[10] R.V. Mangalaraj, J. Mouzon, P. Hedström, C.P. Camurri, S. Ananthakumar, M. Odén, Microwave assisted combustion synthesis of nanocrystalline yttria and its powder characteristics, Powder Technol. 191 (2009) 309–314.
[11] H. Wang, Q. Zhang, H. Yang, H. Sun, Synthesis and microwave dielectric properties of $CaSiO_3$ nanopowder by the sol–gel process, Ceram. Int. 34 (2008) 1405–1408.
[12] J.H. In, H.C. Lee, M.J. Yoon, K.K. Lee, J.W. Lee, C.H. Lee, Synthesis of nano-sized YAG:Eu^{3+} phosphor in continuous supercritical water system, J. Supercrit. Fluids 40 (2007) 389–396.
[13] X.D. Zhang, H. Liu, W. He, J.Y. Wang, X. Li, R.I. Boughton, Novel synthesis of YAG by solvothermal method, J. Cryst. Growth 275 (2005) e1913–e1917.
[14] P. Apte, H. Burke, H. Pickup, Synthesis of yttrium aluminum garnet by reverse strike precipitation, J. Mater. Res. 7 (1992) 706–711.
[15] K.M. Parida, A.C. Pradhan, J. Das, N. Sahu, Synthesis and characterization of nano-sized porous gamma-alumina by control precipitation method, Mater. Chem. Phys. 113 (2009) 244–248.
[16] S.A. Hassanzadeh-Tabrizi, E. Taheri-Nassaj, Economical synthesis of Al_2O_3 nanopowder using a precipitation method, Mater. Lett. 63 (2009) 2274–2276.
[17] B. Djuricic, S. Pickering, Nanostructured cerium oxide: preparation and properties of weakly agglomerated powders, J. Eur. Ceram. Soc. 19 (1999) 1925–1934.
[18] S.T. Aruna, N.S. Kini, K.S. Rajam, Solution combustion synthesis of CeO_2–$CeAlO_3$ nano-composites by mixture-of-fuels approach, Mater. Res. Bull. 44 (2009) 728–733.
[19] L. Vasylechko, A. Senyshyn, D. Trots, R. Niewa, W. Schnelle, M. Knapp, $CeAlO_3$ and $Ce_{1-x}R_xAlO_3$ (R = La, Nd) solid solutions: crystal structure, thermal expansion and phase transitions, J. Solid State Chem. 180 (2007) 1277–1290.
[20] S. Damyanova, C.A. Perez, M. Schmal, J.M.C. Bueno, Characterization of ceria-coated alumina carrier, Appl. Catal. A: Gen. 234 (2002) 271–282.
[21] B.C. Lippens, D.J.H. Boer, Study of phase transformation during calcination of aluminium hydroxides by SAD, Acta Crystallagr. 17 (1964) 1312–1321.
[22] M.G. Scott, Amorphous Metallic Alloys, Butterworths, London, 1983, p. 151.
[23] K.S.W. Sing, D.H. Everett, R.A.W. Haul, L. Moscou, R.A. Pierotti, J. Rouquerol, T. Siemieniewska, Reporting physisorption data for gas/solid

systems with special reference to the determination of surface area and porosity, Pure Appl. Chem. 57 (1985) 603–619.
[24] V.K. LaMer, R. Dinegar, Production and mechanism of formation of monodispersed hydrosols, J. Am. Chem. Soc. 72 (1950) 4847–4854.
[25] Z. Sun, D. Yuan, H. Li, X. Duan, H. Sun, Z. Wang, X. Wei, H. Xu, C. Luan, D. Xu, M. Lv, Synthesis of yttrium aluminum garnet (YAG) by a new sol–gel method, J. Alloys Compd. 379 (2004) L1–L3.
[26] V. Saraswati, G.V.N. Rao, G.V. Rama-Rao, Structural evolution in alumina gel, J. Mater. Sci. 22 (1987) 2529–2534.
[27] D. Sarkar, D. Mohapatra, S. Ray, S. Bhattacharyya, S. Adak, N. Adak, N. Mitra, Synthesis and characterization of sol–gel derived ZrO_2 doped Al_2O_3 nanopowder, Ceram. Int. 33 (2007) 1275–1282.
[28] F. Yen-pei, Preparation of $Y_3Al_5O_{12}$:Ce powders by microwave-induced combustion process and their luminescent properties, J. Alloys Compd. 414 (2006) 181–185.
[29] W. Chen, F. Li, J. Yu, Combustion synthesis and characterization of nanocrystalline CeO_2-based powders via ethylene glycol–nitrate process, Mater. Lett. 60 (2006) 57–62.